# Comparison of Two Optimization-Based Controllers for Feature Tracking SPM Scanning in Dual-Stage Nanopositioners

Yuhe Chang<sup>a</sup>, William S. Nagel<sup>c</sup>, Kam K. Leang<sup>c,1</sup>, and Sean B. Andersson<sup>a,b,2</sup>
<sup>a</sup>Dept. of Mechanical Engineering and <sup>b</sup>Division of Systems Engineering, Boston Univ., Boston, MA 02215
<sup>c</sup>Dept. of Mechanical Engineering, Robotics Center, Univ. of Utah, Salt Lake City, UT, 84112

Abstract -- In this paper, two control methods are investigated for motion tracking of a particular class of trajectories, termed local circular scan (LCS), defined by a non-raster scanning algorithm for scanning probe microscopes. The methods are further developed for multi-axis dual-stage nanopositioning systems. In the first method, the long-range and short-range actuators of a dual-stage system are controlled through model predictive control (MPC) and a linear quadratic tracking controller (LOT), respectively. This architecture lends itself well to applications such as LCS scanning where a distinct highfrequency, low-amplitude signal can be followed entirely by the short-range actuator (SRA) because of the actuator's high bandwidth, but is not easily extended to more generic scenarios. The second method is a discrete linear quadratic controller (LQC) with a cascading reference structure. This scheme is both more general and simpler to implement but does not take advantage of trajectory prior knowledge. Both controllers are validated through simulations on linear models of the planar axes of an experimental dual-stage system, where three planar reference trajectories are selected to evaluate the tracking performances representing different imaging scenarios. Overall, the MPC-receding LQT controller has a better tracking performance for LCS references, likely due to the dedication of the high-frequency sinusoidal components to the SRA and the a priori trajectory information used when calculating the feedforward portion of the control efforts. The MPC-receding LQT controller demonstrates about 30% improvement in the maximum and root-mean-square error over the cascading structure. Tracking is improved further when large steps in the reference signal are desired; the cascading LQC is prone to large overshoot while the MPC-receding LQT reduces the integrated error by more than 70%.

### I. INTRODUCTION

The atomic force microscope (AFM) is a powerful instrument that can resolve material surface properties and dynamics at nanometer-scale, including topology, material moduli, and surface potential [1]–[3]. However, the instrument typically constructs images through raster scanning over a sample pixel-by-pixel, resulting in slow imaging frame rates well below one frame per second on most instruments. Improving these frame rates to achieve video speeds, referred to as high-speed AFM (HS-AFM) [4], generally follows three main approaches: (1) improving system dynamics, (2) employing alternative scan paths, and (3) using advanced controller designs. Herein, the main focus is on a specific approach from the second category, local circular scan (LCS). Figure 1(b) shows a feedback scheme designed for imaging edges (such as cell boundaries) or string-like samples (such

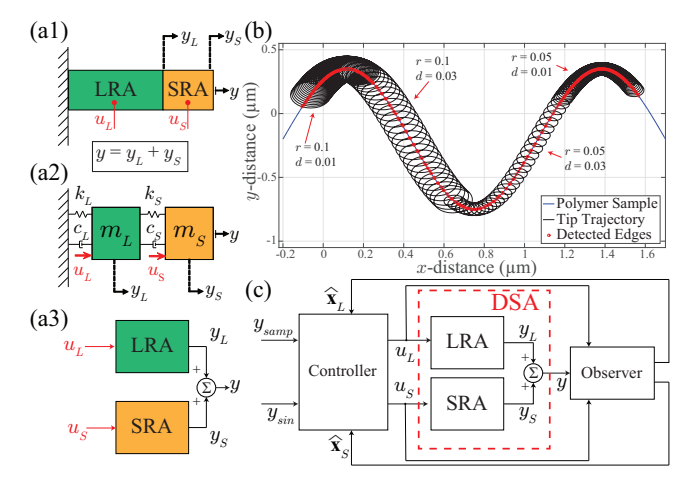


Fig. 1: Dual-stage actuator (DSA) concept: (a1) schematic of the long-range actuator (LRA) and short-range actuator (SRA) connected in series, (a2) lumped-parameter model where the SRA is attached to the LRA mass element, and (a3) dual-input single-output block diagram. (b) Local circular scan (LCS) algorithm concept, where the coarse path is defined by the sample of interest and low amplitude high-frequency circles are executed along the sample. (c) Proposed control structure for a single DSA.

as biopolymers), that has recently emerged for probe-based microscopy [5]. The fundamental idea of LCS is that by driving the cantilever tip in a small circle, measurements can be used in real-time to center the circle on the local position of the sample and to scan the circle along the sample path. This approach focuses the measurements where they are needed, improving imaging rate without requiring faster scanning speeds. The pattern is well suited for a class of actuators known as "dual-stage".

Dual-stage actuators (DSAs) consist of the serial combination of a low-speed, large stroke long-range actuator (LRA) and high-speed short-range actuator (SRA) with a smaller stroke, as shown in Fig. 1(a1). The lumped-parameter and input-output structure are shown in Fig. 1(a2) and (a3), respectively. The combined efforts of these two actuators allows for the full dual-stage system to exhibit simultaneously large range, high bandwidth, and fine precision [6]. This concept is largely associated with hard disk drives (HDDs), which consist of a long-range voice coil motor (VCM) moving a small piezoelement (PZT) that is attached to the read/write head [7]. Other applications of dual-stage systems include optic alignment systems [8], measuring machines [9], and probe-based microscopes [6], [10].

 $<sup>^1</sup>$ kam.k.leang@utah.edu;  $^2$ sanderss@bu.edu

A wide variety of controllers have been developed for dual-stage systems. Examples include proportional-integral-derivative (PID) controllers [11], complementary filters [8], or combinations thereof. More advanced controller architectures have demonstrated improvement in the positioner's performance, for example when performing nonlinear filtering of references based on the DSA range limitations rather than frequency content [10], or through direct compensation of nonlinear effects such as hysteresis [12]. Furthermore, optimal controllers have been shown to exhibit good performance, such as robust  $H_{\infty}$  control [6] and model predictive control (MPC) [13].

Herein, two optimal controllers are designed for a dualinput single-output (DISO) system based on the basic architecture illustrated in Fig. 1(c). This design is specifically tailored to LCS trajectories. The first approach divides the LRA and SRA roles according to the LCS scan pattern. Specifically, the SRA is dedicated to the low-amplitude, high-frequency sinusoidal elements defining the repeated circle; for this, a receding-horizon, linear quadratic tracking (LQT) controller is exploited. The path of the sample is then tracked using MPC. The second is a cascading linear quadratic controller (LQC) with an augmented feedforward control term to remove a priori reference input knowledge requirements. To compare the relative performance of these approaches, simulations based on models of an experimental dual-stage nanopositioner are performed. The main contributions of this work are the development of the MPC-receding LQT control paradigm, as well as the simulation performance comparisons of the controllers to help guide future LCS design and HS-AFM implementation.

The remainder of this paper is organized as follows. Derivations of the proposed MPC-receding LQT controller are provided in Section II; this section also includes details of the cascading LQC design, although a more thorough explanation is available in [14]. Section III describes the modeling of an experimental multi-axis dual-stage nanopositioner and the simulations selected to compare control performances. A discussion of the simulation results is provided in Section IV followed with concluding remarks.

# II. CONTROLLER DESIGN

### A. DSA Model and Observer

Dual-stage systems are multi-input, single-output (MISO) systems with two inputs and a single output. Often, the total dynamics are treated as separate linear time invariant (LTI) single-input, single-output (SISO) systems, where interplay dynamics between the actuators are ignored. These actuators can be modeled by general discrete-time SISO linear state-space equations, where L denotes the LRA and S denotes the SRA. These are then combined in the total dual-stage system dynamics given by

$$\begin{bmatrix} \boldsymbol{x}_L(k+1) \\ \boldsymbol{x}_S(k+1) \end{bmatrix} \! = \! \begin{bmatrix} A_L & \mathbf{0} \\ \mathbf{0} & A_S \end{bmatrix} \begin{bmatrix} \boldsymbol{x}_L(k) \\ \boldsymbol{x}_S(k) \end{bmatrix} + \begin{bmatrix} B_L & \mathbf{0} \\ \mathbf{0} & B_S \end{bmatrix} \begin{bmatrix} u_L(k) \\ u_S(k) \end{bmatrix},$$

$$y(k) = y_L(k) + y_S(k) = \begin{bmatrix} C_L & C_S \end{bmatrix} \begin{bmatrix} \boldsymbol{x}_L(k) \\ \boldsymbol{x}_S(k) \end{bmatrix}.$$
 (1)

This model can be expanded to include more intricacies, such as nonlinearities and coupling effects. For convenience, these effects are not considered to allow for a more direct comparison of the controllers based on linear system dynamics.

In previous work [15], the observability and controllability of dual-stage systems is established. It is necessary to develop an observer to provide estimates of the actuator states in order to deploy controllers for the LRA and SRA. Herein, a standard discrete Luenberger observer is used that takes the form:

$$\hat{\boldsymbol{x}}(k+1) = [A - LC]\hat{\boldsymbol{x}}(k) + B\boldsymbol{u}(k) + L\boldsymbol{y}(k), \quad (2)$$

where A, B, and C represent the concatenated DSA state-space matrices from (1), and  $\hat{x}$  and u are the column vectors of both actuators state estimates and input variables, respectively. The observer gain L is designed such that the eigenvalues of A-LC are much faster than those of the DSA dynamics. From the observer, the estimated outputs can be defined as

$$\hat{y}_L = C_L \hat{\boldsymbol{x}}_L, \quad \hat{y}_S = C_S \hat{\boldsymbol{x}}_S. \tag{3}$$

# B. MPC and Receding LQT

Combined with the LCS scanning pattern, the LRA attempts to track an unknown sample path being imaged. In real systems, there are physical constraints, including input and output boundaries. The input limits for both actuators are limited by the voltage signal provided to the amplifiers of the dual-stage actuators, while the output boundaries are determined by the physical stroke achievable by each actuator. To account for these, an MPC design is used.

MPC uses a discrete time model of the dynamic system to predict the system performance in a predefined time horizon in the future in order to arrive at the optimal control action subject to the constraints at each instant of time [16]. In this work, MPC is applied to the LRA to achieve output tracking of the sample trajectory. The corresponding optimal control problem is

$$\min_{u_L} \frac{1}{2} \sum_{i=0}^{N_p} ||(\hat{y}_L(k+i) - r_L(k+i))||_Q^2 + \sum_{i=0}^{N_m - 1} ||u_L(k+i)||_R^2$$

subj. to 
$$u_{min} \le u_L(k+i) \le u_{max}, k = 0, 1, \dots, N_m - 1,$$
  $y_{L_{min}} \le y_L(k+i) \le y_{L_{max}}, k = 0, 1, \dots, N_p.$ 

where k is the current step,  $N_p$  is the length of the prediction horizon,  $N_m$  is the length of the control horizon  $(N_m \leq N_p)$ , and  $r_L$  is the reference trajectory for the LRA, taken to be the path of the sample being tracked using LCS. The notation  $\|\cdot\|_M$  refers to the norm  $\|x\|_M = x^T M x$ . Solving this quadratic problem at each point in time gives the control to be applied to the LRA. Note that while in practice the sample trajectory  $r_L(t)$  is unknown in advance, it can be predicted locally based on recent data (see [17]).

**Remark**: The authors recognize that this is a simple formulation for MPC tracking. Including features such as

feasibility of the desired trajectory with respect to system constraints, terminal costs or constraints to guarantee stability, and including the state in the cost function together with the impact of the observer are subjects of ongoing work.

In the proposed design, the SRA follows the circular portion of the LCS trajectory. Since this circular path is entirely designed by the user, it is assumed to be selected so as to satisfy all constraints of the actuator and thus those constraints are not considered in the control design. A linear quadratic output tracking controller (LQT) to track the repetitive motion is used. The concept of LQT is an extension of the linear quadratic regulator (LQR) and is used when the system output needs to track a desired reference trajectory and reject a given disturbance with an optimized cost function. Typically, LQT control is applied over a finite time horizon and uses *a priori* knowledge of the signal to be tracked [18]. The cost function in discrete time is

$$\min_{u_S} \frac{1}{2} \|C\hat{x}_S(N) - r_S(N)\|_{\bar{P}}^2 
+ \frac{1}{2} \sum_{k=0}^{N} (\|C\hat{x}(k) - r(k)\|_Q^2 + \|u(k)\|_R^2),$$

where  $r_S$  is a sinusoidal reference signal and P, Q, and R, are scalar weights for tracking and input efforts. Following standard derivations, the state feedback control law is

$$u^*(k) = -K_{fb}(k)\hat{x}(k) + K_{ff}(k)v(k+1). \tag{4}$$

The gain matrices and feedforward terms are found by solving the matrix Riccati equation and vector difference equation over the finite time horizon using

$$K_{fb}(k) = [B^T P(k+1)B + R]^{-1} B^T P(k+1)A,$$
 (5a)  

$$P(k) = A^T P(k+1)[A - BK_{fb}(k)] + C^T QC,$$
 (5b)  

$$\mathbf{v}(k) = [-BK_{fb}(k)]^T \mathbf{v}(k+1) + C^T Qr_S(k),$$
 (5c)  

$$K_{ff}(k) = [B^T P(k+1)B + R]^{-1} B^T,$$
 (5d)

with  $P(N) = C^T \bar{P}C$  and  $\mathbf{v}(N) = C^T \bar{P}r(N)$ .  $K_{fb}$  is the optimal feedback gain, while  $K_{ff}$  is a feedforward gain that depends on the auxiliary sequence  $\boldsymbol{v}$  determined from the reference signal via a difference equation (note P and  $\boldsymbol{v}$  are backward difference equations). Clearly, the solution depends on knowing  $r_S(N)$  and the horizon, N. In practice, however, while the reference is a given sinusoid, there is no pre-defined terminal time N. To overcome this, a receding time horizon LQT design is used, solving over an N-step horizon, applying the first control value, and then repeating.

#### C. Cascading LQC

To contrast the proposed MPC and receding LQT controller, a control architecture that is derived from optimality conditions but generalized to be implementable without *a priori* trajectory knowledge is also used. This controller, first presented in [14], derives individual linear quadratic compensators for the LRA and SRA, but the actuator references effectively cast them into a cascading form. Specifically, the

LRA attempts to track the entire reference trajectory for that axis, while the SRA tracks the LRA's error, written as

$$r_L(k) = y_{des}(k), \quad r_S(k) = y_{des}(k) - \hat{y}_L(k),$$

where  $r_{L,S}$  denotes the trajectory that each actuator is tracking. In the LCS setting, the single reference  $y_{des}$  is the sum of the sinusoidal component to generate the circular scan and the (estimate) of the sample path being tracked.

The LQC laws for the actuators are determined through the same formulation as the LQT controller discussed prior, but with two modifications for easier implementation. First, the steady-state solution of the feedback gain is used, solved from the discrete algebraic Riccati equation. Second, the feedforward term in (5c) is solved forward in time assuming zero initial conditions,

$$\mathbf{v}_{j}(k+1) = [A_{j} - B_{j}K_{j,fb}]\mathbf{v}_{j}(k) + C_{j}^{T}Q_{j}r_{j}(k),$$
 (6)

where  $j \in \{L, S\}$ . This result is an implementation of LQT where the feedforward term sacrifices optimality for the capability of tracking an arbitrary reference trajectory without pre-computation.

#### III. PERFORMANCE COMPARISON

#### A. Experimental System

The two controllers outlined in the previous section are compared below through simulations on models of an experimental multi-axis dual-stage nanopositioner, designed specifically for LCS and other similar algorithms [19]. This device, shown in Fig. 2(a), consists of two planar piezostack actuators interfaced into a mechanical flexure mechanism to guide and amplify their motion. The center platform of this mechanism houses a single three-axis shear actuated piezoelement which serves as the SRA for both the x- and y-axes. An aluminum cap, the output port of the positioner, is affixed to the top of this shear actuator. Samples can be attached to this cap and the faces are used as the measurement surfaces for capacitive sensors.

Linear models of the planar actuators are found by fitting dynamic models to frequency response data obtained via swept sine measurements taken with low input voltages to mitigate hysteresis effects; these are shown in Fig. 2(b). Fits are empirically made to the measured data rather than through first principles, as the LRA flexure mechanism exhibits additional resonance shapes before the SRA resonance is excited. The LRA dynamics are modeled using a  $3^{rd}$  order system with a dominant resonance at approximately 1.4 kHz, while the SRA dynamics are modeled as a  $15^{th}$  order system with resonances and anti-resonances predominantly between 1.4 kHz to 40 kHz. The LRA frequency response is from 100 Hz to 3 kHz and the SRA responses are measured from 1 kHz to 20 kHz, so creep effects are negligible. Note that the effect of nonlinearities such as hysteresis and creep are ignored in order to focus on a comparison of the two control techniques in a simpler, linear setting.

Input and output boundaries, which are used in the MPC formulations and incorporated as constraints in the simulation models, are determined from the nanopositioner stroke

TABLE I: Controller parameters used for simulation.

		P	Q	R
MPC-receding LQT	MPC		1	1
	LQT	0.25	25,000	1
Cascading LQC	LRA		125,000	1
	SRA		3,750	1

length and the electronics used to power the actuators. The LRAs for both axes have a maximum displacement of  $\pm 8~\mu m$  while the SRAs' displacements have maximum values of  $\pm 0.35~\mu m$ . Input voltages for all actuators are based on the inputs to the high voltage amplifiers for the stages and were set to  $\pm 10$  volts. These limits are explicitly considered in the controller formulations for the MPC-receding LQT design and are experienced by both compensation approaches through saturation calculations before the linear dynamic models. The horizons for the MPC controller are set to  $N_p=N_m=10$  and the receding-horizon LQT horizon is set to N=10.

#### B. Simulation Details

The controllers described in Sec. II are applied to the actuator models described above through simulation using the parameter values in Table I. These values are chosen through trial and error to achieve good performance. To highlight potential conditions where these controllers may be beneficial, three trajectory scenarios are explored. These consisted of different periodic coarse 2D paths with high-frequency circular scanning as described for the LCS algorithm. Thus all three scenarios examined here have the fine reference trajectories

$$r_{x,SRA}(k) = 0.1\cos(2\pi 2000k\Delta t),$$
 (7a)

$$r_{y,SRA}(k) = 0.1\sin(2\pi 2000k\Delta t),$$
 (7b)

where time step  $\Delta t$  is taken to be  $\Delta t = 2.5~\mu s$  (400 kHz). Note that while this time step is challenging for MPC, there are existing results in implementing MPC at these rates (see, e.g. [20]).

The coarse path for Scenario I consists of a repeating circle pattern with a radius of 5  $\mu$ m, followed at a rate of 20 circles per second. Scenario II follows a string-like path (e.g., a biopolymer strand), moving end-to-end along the strand five times every second. The last coarse trajectory consists of several 1–2  $\mu$ m steps, where each step can be interpreted as a separate biopolymer strand to be scanned with the LCS algorithm. The resulting 2D path resembles the

TABLE II: Tracking errors for MPC-receding LQT and cascading LQC for the *y*-axis of the 2D trajectories.

Trajectory	Controller	$e_{max}$	$e_{rms}$	$e_1$
		(µm)	(µm)	(µm)
Circle	MPC-receding LQT	0.0318	0.0186	0.0165
	Cascade LQC	0.0429	0.0261	0.0233
String-like	MPC-receding LQT	0.0286	0.0181	0.0163
	Cascade LQC	0.0455	0.0257	0.0231
Staircase	MPC-receding LQT	2.0019	0.0544	0.0134
	Cascade LQC	2.3003	0.1545	0.0464

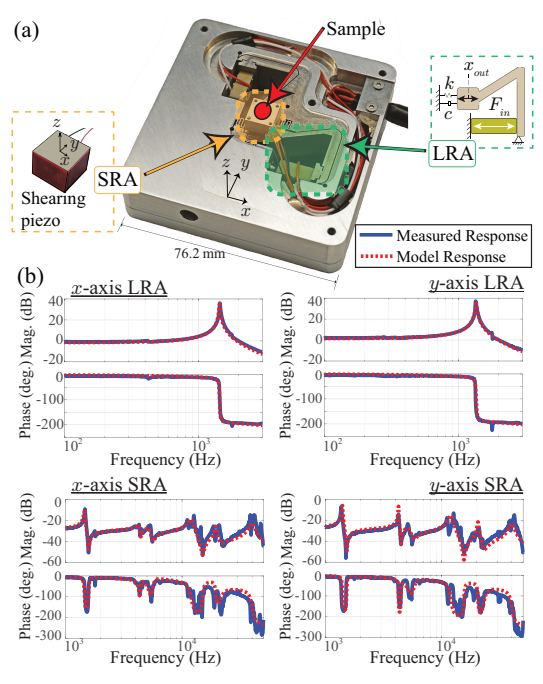


Fig. 2: (a) Experimental multi-axis dual-stage nanopositioner modeled for controller performance and (b) the measured frequency responses and linear models for the *x*-axis and *y*-axis LRA and SRA behaviors.

steps of a "staircase", so this moniker will be used herein. These trajectories and the tracking performances of the MPC-receding LQT and cascading controllers are shown in Fig. 3.

# C. Results

Due to initial conditions mismatch arising from the simulation environment, the cascading controller has a large initial error. To avoid skewing the metrics due to the initial transients, all shown results are after the initial convergence period. Thus, all plots and tables show results only after the controllers reach the initial steady state. Note that the staircase pattern re-excites these transients as part of the trajectory and those transients are quantified in the metrics of performance.

Both proposed controllers have good tracking results as shown in Table II. Three metrics are included to quantify the error of a single axis. Note that due to space limitations, results are only shown for the y-axis. Results in the x-direction are similar. The maximum error  $e_{max}$  and root-mean-square (RMS) error  $e_{rms}$  are calculated using

$$e_{max} = \max_{k} |e(k)|, \tag{8}$$

$$e_{rms} = \left(\frac{1}{N_e} \sum_{k=0}^{N_e} e(k)^2\right)^{1/2},$$
 (9)

where  $N_e$  is the number of samples for a period of the error signal. In addition, the normalized  $l_1$ -norm of the error over one period is reported, given by

$$e_1 = \frac{1}{N_e} \sum_{k=0}^{N_e} |e(k)|. \tag{10}$$

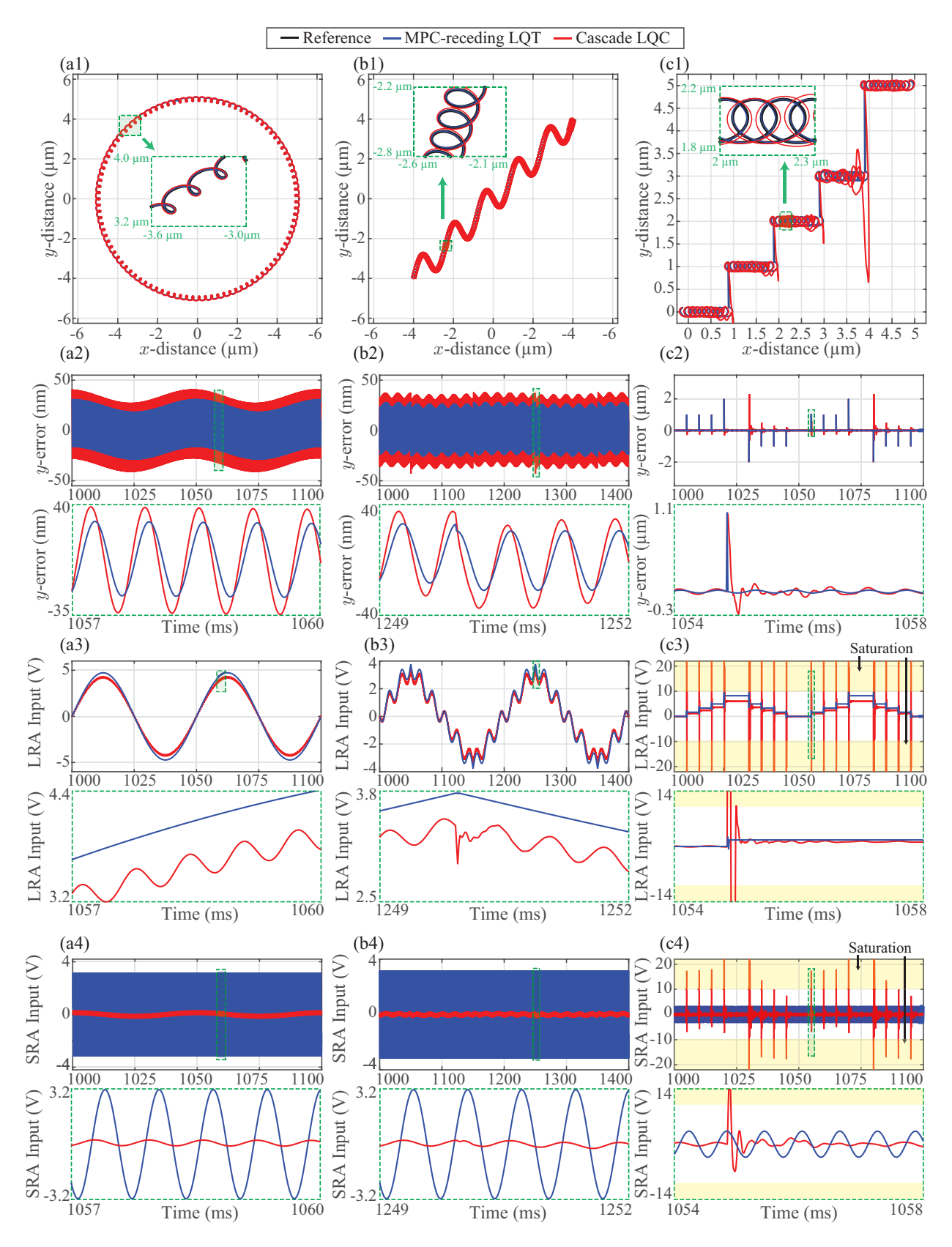


Fig. 3: Simulation results for the proposed MPC-receding LQT controller and the cascading LQC designs. 2D LCS trajectory tracking results are shown for the (a1) circular, (b1) string-like, and (c1) staircase paths. Time response results are also included, where (a2)–(c2) highlight error for the y-axis of the DSA, (a3)–(c3) depict control efforts for the y-axis LRA while (a4)–(c4) show the SRA efforts. For all plots, black is the reference, blue are the MPC-receding LQT results, and red is the cascading LQC results. Green dashed borders indicated zoomed in results, and yellow sections refer to control efforts that are saturated when applied.

Plots of the system's joint output, as well as single-axis outputs, errors, and control efforts are shown in Fig. 3.

#### IV. DISCUSSION

The 2D tracking and y-axis time response plots in Fig. 3(a1)-(a4) illustrate that the MPC-receding LOT and cascading LQC both track well for high, with maximum and RMS error values less than 1% of the total amplitude of the circular trajectory. Table II catalogs these errors, as well as those for the other two trajectory scenarios. While both controllers perform well, the MPC-receding LQT controller improves upon the cascading numbers by 25-37% for these maximum and RMS errors, indicating a notable improvement over the causal controller. Note that the cascading LQC on the SRA exerts significantly lower effort than the recedinghorizon LOT controller, shifting that effort to the LRA. This likely contribute to the lower performance. Similarly, in Scenario II (Fig. 3(b1)-(b4)), the MPC-receding LQT tracked the string-like path better than the cascade LQC for these same metrics. One particular point to note is that the turnaround point at the ends of the path resulted in bigger spikes in error for the cascading controller, contributing to the larger maximum error observed in these results.

Scenario III, Fig. 3(c1)-(c4), the staircase trajectory, highlights the clearest differences in the controller performances. The large transients of the cascading controller occur because the cascading controller does not predict these future transitions. To minimize its cost function, the cascading controller will then drive large control signals to bring the DSA quickly back to the sample trajectory, see Fig. 3(c3)-(c4). Therefore, at each step point, the cascading controller yielded large control signals which surpassed the equipment voltage constraints. Table II also indicates that the maximum and RMS errors for this path were much larger than the other scenarios, due to this instantaneous jump in the reference signal. Thus a more indicative metric to consider for this scenario is the  $L_1$ -norm in (10). This shows that while both controllers were still effective for this scenario, the MPCreceding LQT compensator shows 71% reduction in the error signal's integral, demonstrating the utility of the noncausal calculations in scenarios with large step changes in the reference signal.

#### V. CONCLUSIONS

This paper compared two control strategies for a dualstage scanning system with a focus on trajectories relevant to local circular scanning for high-speed imaging in AFM. The first controller divided the LRA and SRA according to the LCS algorithm, applying an MPC to the LRA to achieve sample trajectory tracking and a receding LQT to the SRA to follow the repetitive motion. This was compared to an optimal cascading LQC that eliminated *a priori* requirements for trajectory tracking. The comparison between these two controllers revealed that the performance of the MPC-receding LQT for LCS trajectories outperformed the cascade controller, especially for the staircase path. Note that the conclusions in this paper are not expected to hold for generic trajectories but are specific to the LCS algorithm. In future work, the MPC approach will be tested on a physical dual-actuation stage designed for high-speed AFM.

#### ACKNOWLEDGEMENTS

This work was supported in part by NSF under grants No. DBI 1461593 and CMMI 1537983 and 1537722, as well as NIH through NIGMS-1R01GM117039-01A1.

#### REFERENCES

- D. J. Muller, "AFM: A nanotool in membrane biology," *Biochemistry*, vol. 47, no. 31, pp. 7986–7998, 2008.
- [2] S. Liu and Y. Wang, "Application of AFM in microbiology: a review," Scanning, vol. 32, no. 2, pp. 61–73, 2010.
- [3] K. Haase and A. E. Pelling, "Investigating cell mechanics with atomic force microscopy," *Journal of The Royal Society Interface*, vol. 12, no. 104, p. 20140970, 2015.
- [4] T. Ando, "High-speed atomic force microscopy coming of age," Nanotechnology, vol. 23, no. 6, p. 062001, 2012.
- [5] B. Hartman and S. B. Andersson, "Feature tracking for high speed AFM imaging of biopolymers," *International Journal of Molecular Sciences*, vol. 19, no. 4, p. 1044, 2018.
- [6] T. Tuma, W. Haeberle, H. Rothuizen, J. Lygeros, A. Pantazi, and A. Sebastian, "Dual-stage nanopositioning for high-speed scanning probe microscopy," *IEEE/ASME Transactions on Mechatronics*, vol. 19, no. 3, pp. 1035–1045, 2014.
- [7] Y. Li and R. Horowitz, "Mechatronics of electrostatic microactuators for computer disk drive dual-stage servo systems," *IEEE/ASME Trans*actions on Mechatronics, vol. 6, no. 2, pp. 111–121, 2001.
- [8] Y. K. Yong, S. P. Wadikhaye, and A. J. Fleming, "High speed singleand dual-stage vertical positioners," *Review of Scientific Instruments*, vol. 87, no. 8, p. 085104, 2016.
- [9] M. Ringkowski, E. Arnold, and O. Sawodny, "Optimal reference allocation of dual-stage measuring machines," in *IEEE/ASME Inter*national Conference on Advanced Intelligent Mechatronics (AIM), pp. 1362–1367, 2020.
- [10] A. Mitrovic, W. S. Nagel, K. K. Leang, and G. M. Clayton, "Closed-loop range-based control of dual-stage nanopositioning systems," *IEEE/ASME Transactions on Mechatronics (published online)*, DOI: 10.1109/TMECH.2020.3020047, 28-July-2020.
- [11] A. Elfizy, G. Bone, and M. Elbestawi, "Design and control of a dual-stage feed drive," *International Journal of Machine Tools and Manufacture*, vol. 45, no. 2, pp. 153–165, 2005.
- [12] J. Zheng, H. Lu, Q. Wei, X. Chen, and Z. Li, "Dual-piezoelectric ceramic micro-positioning control based on the modified prandtlishlinskii model," in *IEEE International Conference on Information* and Automation (ICIA), pp. 2036–2040, 2016.
- [13] M. A. Rahman, A. A. Mamun, K. Yao, and Y. Daud, "Discrete-time model predictive control for head-positioning servomechanism in a dual-stage hard disk drive," in *IEEE International Conference on Mechatronics and Automation*, pp. 8–13, 2014.
- [14] W. S. Nagel and K. K. Leang, "Cascading structure linear quadratic tracking control for dual-stage nanopositioning systems," in *IEEE American Control Conference (ACC)*. pp. 70–75, 2020.
- [15] Y. Chang and S. B. Andersson, "Observer-based control of a dualstage piezoelectric scanner," in ASME Dynamic Systems and Control Conference (DSCC). p. V003T19A008, 2019.
- [16] A. Bemporad and M. Morari, "Robust model predictive control: A survey," in *Robustness in Identification and Control*, A. Garulli and A. Tesi, Eds. Springer, London, pp. 207–226, 1999.
- [17] P. Huang and S. B. Andersson, "Note: Fast imaging of DNA in atomic force microscopy enabled by a local raster scan algorithm," *Review of Scientific Instruments*, vol. 85, no. 6, p. 066101, 2014.
- [18] B. D. O. Anderson and J. B. Moore, Linear Optimal Control, Prentice-Hall, 1971.
- [19] W. S. Nagel and K. K. Leang, "Design of a dual-stage, three-axis hybrid parallel-serial-kinematic nanopositioner with mechanically mitigated cross-coupling," in *IEEE/ASME International Conference on Advanced Intelligent Mechatronics (AIM)*. pp. 706–711, 2017.
- [20] I. McInerney, G. A. Constantinides, and E. C. Kerrigan, "A survey of the implementation of linear model predictive control on FPGAs," *IFAC-PapersOnLine*, vol. 51, no. 20, pp. 381–387, 2018.